Journal of Industrial and Engineering Chemistry 79 (2019) 204–209

Contents lists available at ScienceDirect

Journal of Industrial and Engineering Chemistry

journal homepage: www.elsevier.com/locate/jiec

# Microporous waste charcoals for redox-mediated supercapacitors

Jong Chan Hyun, Jin Hwan Kwak, Young Soo Yun*

*Department of Chemical Engineering, Kangwon National University, Samcheok 245-711, South Korea*

ARTICLE INFO

*Article history:*
Received 23 January 2019
Received in revised form 8 June 2019
Accepted 22 June 2019
Available online 28 June 2019

*Keywords:*
Activated carbon
Porous carbon
Electrodes
Charcoal
Supercapacitor

ABSTRACT

The energy density of supercapacitors could be improved significantly using microporous carbon-based materials (MP-CMs) with multitudinous redox-active heteroatoms through the hybrid charge storage behaviors of both pseudocapacitance and electrochemical double layer capacitance in a redox-mediated aqueous electrolyte system. Waste-derived MP-CMs were prepared using a simple activation process and used as high-performance electrode materials for redox-mediated supercapacitors, showing a high specific capacitance of 512 F $g^{-1}$ and a reasonable rate and cycling performance.



## Introduction

Supercapacitors can deliver high power with stable cycles owing to their unique charge storage characteristics based on the electrochemical double layers (EDLs), having attracted considerable attention in energy storage fields [1,2]. On the other hand, the relatively poor energy density of supercapacitors (<10 Wh $kg^{-1}$) compared to conventional rechargeable batteries (200 Wh $kg^{-1}$) has limited their applications, which depends strongly on the electrode properties: the electroactive surface area of the electrode and the charge separation distance between the ion and electrode [3]. In addition, pseudocapacitive charge storage on redox-active heteroatoms of the electrode surface can increase the capacitance. Therefore, electrode design with a high surface area, effective pore structure, and numerous redox-active heteroatoms is one of the key issues for achieving high energy supercapacitors [1–8]. Zhao et al. reported that nitrogen-containing porous carbon with a relatively low specific surface area of <600 $m^2$ $g^{-1}$ can deliver a high specific capacitance of 220 F $g^{-1}$ in a 6 mol KOH electrolyte [7]. In addition, Hulicova-Jurcakova et al. showed the combined effects of pseudocapacitance from nitrogen and oxygen functional groups. These results highlight the strong effects of the pseudocapacitive charge storage behaviors on carbon-based electrode materials. Nevertheless, several carbon-based materials even possessing specific surface areas above 3000 $m^2$ $g^{-1}$ and sub-nanometer-scale pores as well as a large amount of heteroatoms showed unsatisfactory specific capacitance [7–15]. A recent study reported that the specific capacitance of supercapacitors can be increased dramatically using a redox-active electrolyte [16–22]. Wu et al. reported that a high specific energy of 20 Wh $kg^{-1}$ was achieved in a p-phenylenediamine (PPD) and KOH mixture electrolyte [18]. Zhang et al. reported that in a similar mixture electrolyte, a carbon-based electrode showed a high specific capacitance of approximately 500 F $g^{-1}$, which is about 4.1 times higher than that in a KOH electrolyte [22]. The steep enhancement of the specific capacitance originated from both the redox reaction of PPD dissolved in the electrolyte and charge storage based on the formation of EDLs. Therefore, high energy supercapacitors could be achieved through the hybrid effects of the exquisite electrode design and redox-active electrolyte.

In this study, microporous carbon-based materials (MP-CMs) were prepared by the simple heating of waste charcoal (WCs) with KOH for use as an electrode in supercapacitors. The MP-CMs prepared using 400 wt.% KOH had a high specific surface area of 1784.2 $m^2$ $g^{-1}$ as well as numerous redox-active heteroatoms on their surface, leading to high electrochemical performance. In particular, in the redox-mediated electrolyte, MP-CMs showed a high specific capacitance of 512 F $g^{-1}$ at 1 A $g^{-1}$ by both pseudocapacitance and electrochemical double layer (EDL) capacitance, which is approximately two times higher than that in conventional aqueous electrolytes.

## Experimental

### *Preparation of MP-CMs*

WCs were obtained from a Korean restaurant in Incheon. A 10 g sample of waste charcoal was ground and mixed with 10, 20, 40, or 60 g of KOH in a mortar. The mixture was heated in a furnace to 800 °C and held at that temperature for 2 h. A heating rate of 10 °

* Corresponding author.
*E-mail address:* ysyun@kangwon.ac.kr (Y.S. Yun).

https://doi.org/10.1016/j.jiec.2019.06.036
1226-086X/

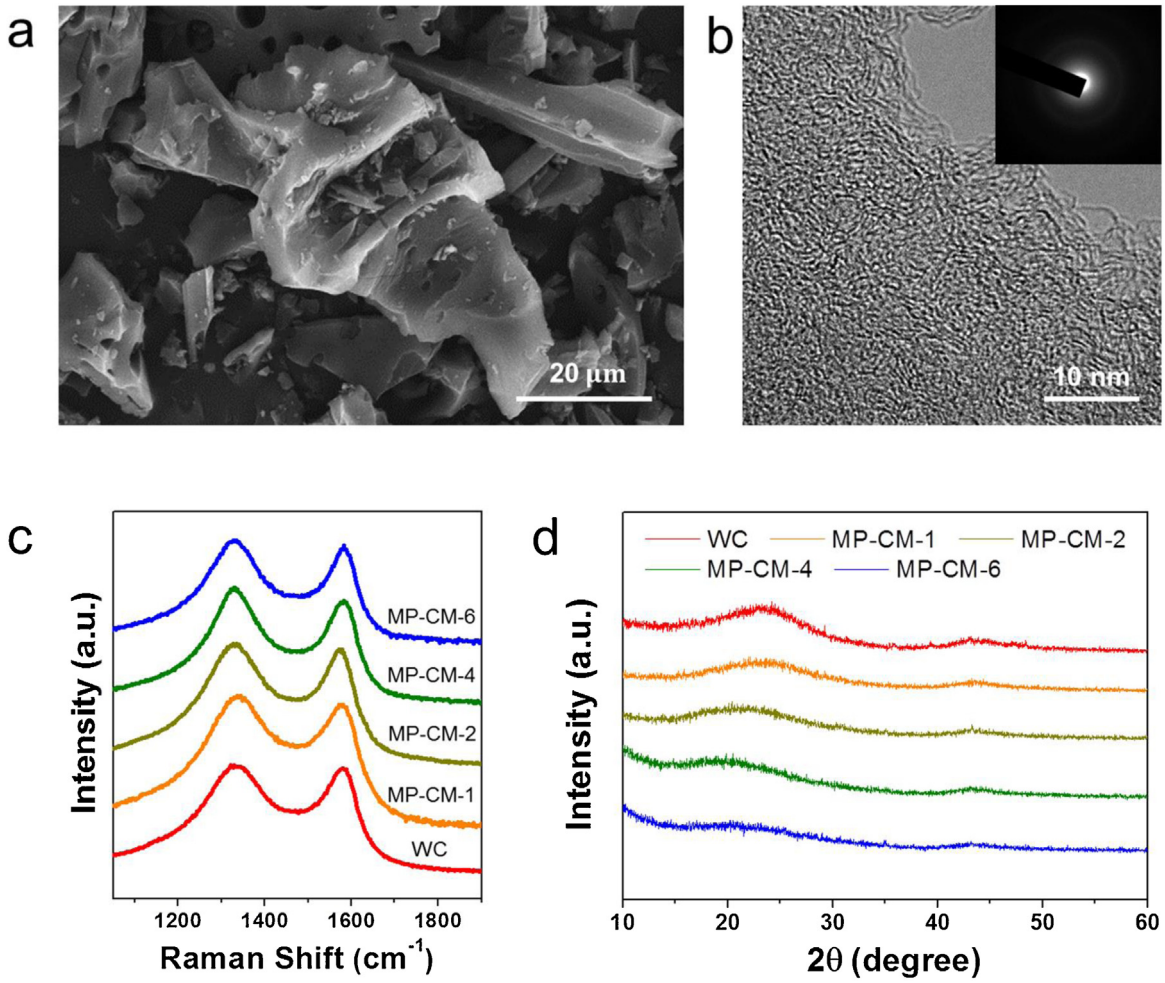


**Fig. 1.** (a) FE-SEM and (b) FE-TEM images of MP-CM-4. (c) Raman spectra and (d) XRD patterns of WC and MP-CMs.

C $min^{-1}$ and Ar flow of 200 mL $min^{-1}$ were applied for the heating process. The resulting materials were washed several times with ethanol and water, and dried in an oven at 60 °C. The produced samples are called MP-CM-1, -2, -4, and -6 according to the KOH to waste charcoal ratio.

*Characterization*

The morphology of the samples was characterized by field-emission scanning electron microscopy (FE-SEM, S-4300, Hitachi, Japan) and field-emission transmission electron microscopy (FE-TEM, JEM2100 F, JEOL, Tokyo, Japan). The Raman spectra were recorded using a continuous-wave linearly polarized laser (514.5 nm wavelength, 2.41 eV, 16 mW power). The laser beam was focused by a 100× objective lens, resulting in a ~1 μm diameter spot. X-ray diffraction (XRD, Rigaku DMAX 2500) was performed using Cu–Kα radiation with a wavelength λ = 0.154 nm at 40 kV and 100 mA. X-ray photoelectron spectroscopy (XPS, PHI 5700 ESCA, USA) was used to examine the surface chemical properties of the samples. The pore structure was characterized by nitrogen

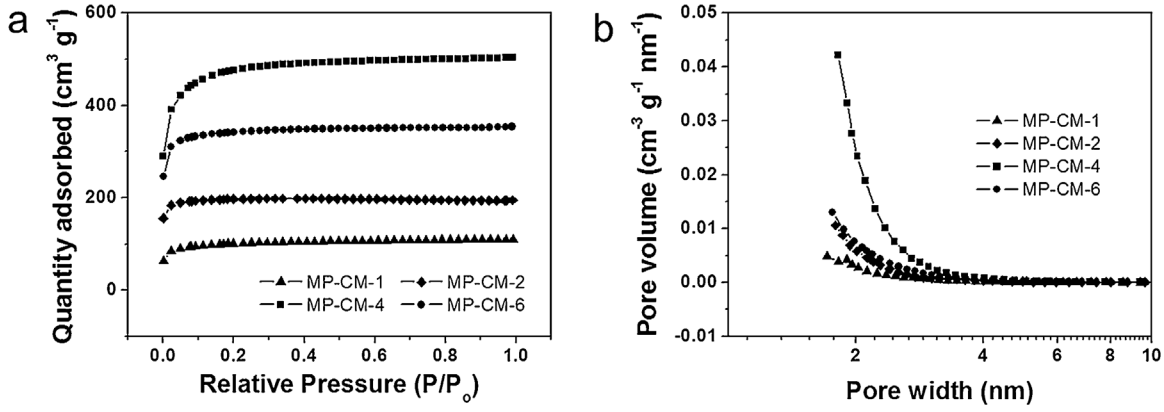


**Fig. 2.** (a) Nitrogen adsorption and desorption isotherm curves of MP-CMs, and (b) pore size distributions of MP-CMs.

**Table 1**
Textural properties of MP-CMs.

| Sample | Textural properties | | |
|---|---|---|---|
| | $S_{BET}$ ($m^2 g^{-1}$)[a] | Pore volume ($cm^3 g^{-1}$) | Pore width (nm)[b] |
| MP-CM-1 | 377.2 | 0.299 | 1.3 |
| MP-CM-2 | 786.2 | 0.394 | 1.7 |
| MP-CM-4 | 1784.2 | 0.877 | 3.2 |
| MP-CM-6 | 1324.1 | 0.568 | 1.9 |

[a] $S_{BET}$: BET specific surface area.
[b] Pore width: Adsorption average pore width characterized by BET method.

adsorption and desorption isotherm tests using a surface area and porosimetry analyzer (Tristar, Micromeritics, USA) at −196 °C.

*Electrochemical characterization*

The electrochemical properties of the samples were characterized by cyclic voltammetry (CV) and chronopotentiometry (PGSTAT302 N, Autolab). Ag/AgCl and Pt wire were used as the reference and counter electrodes, respectively. A 6 M KOH aqueous solution and 2 M KOH aqueous solution containing 0.05 M PPD were used as the electrolytes. The three electrode system was tested in a beaker cell. The working electrodes were prepared by adding 5 wt. % polytetrafluoroethylene (PTFE, Sigma-Aldrich, 60 wt.% dispersion in $H_2O$) to the active material. The active samples and PTFE were mixed into a paste using a mortar and pestle, rolled into uniformly thick sheets (thicknesses ranging from 40 to 50 mm), and punched into 1 cm square electrodes. The loading of the active electrode was 3–4 mg after drying overnight at 100 °C. The specific capacitance was determined from galvanostatic measurements using the following equation:

$$C = \frac{4I_{cons}}{mdV/dt} \quad (1)$$

where $I_{cons}$ is the (constant) current, $m$ is the total mass of both carbon electrodes, and $dV/dt$ was calculated from the slope of the discharge curve over the voltage window.

## Results and discussion

Fig. 1(a) presents the morphologies of MP-CM-4. The debris of MP-CM-4 was a micrometer-scale with an irregular shape. High-resolution FE-TEM showed that MP-CMs-4 have an amorphous carbon structure without long-range graphitic carbon ordering (Fig. 1(b)). The selective area diffraction pattern also supports the non-crystalline structure of the MWCs-4 (Inset of Fig. 1(b)). The microstructures of the MP-CMs were characterized further by Raman spectroscopy and XRD (Fig. 1(c) and (d)). The Raman spectra exhibited *D* and *G* bands, which correspond to the disorder in the $A_{1g}$ breathing mode of the six-fold aromatic ring near the basal edge and the hexagon structure related to the $E_{2g}$ vibration mode of the $sp^2$-hybridized C atoms, respectively (Fig. 1(c)) [23]. Therefore, the presence of the *D* and *G* bands indicates the development of a poly-hexagonal carbon structure.The surface properties of MP-CMs were characterized In addition, the *D* and *G* bands were fused with each other, indicating that the carbon structure includes a large number of defective structures (Fig. 1(c)). The Raman spectra of all the samples showed a similar *D* to *G* intensity ratio, showing that the sizes of the ordered hexagonal carbon domains are similar on a few nanometer-scale regardless of the activation process (Fig. 1(c)). In XRD patterns, a very broad graphite (002) peak was observed in WC, which became broader with increasing activation agents. These results show that MP-CMs have poor stacking order.

The pore structure of the MP-CMs was characterized by nitrogen adsorption and desorption isotherm curves, as shown

**Table 2**
Surface properties of MP-CMs obtained from XPS.

| Sample | Atomic ratio (at.%) | | | |
|---|---|---|---|---|
| | C | O | N | S |
| MP-CM-1 | 88.3 | 8.0 | 1.6 | 2.1 |
| MP-CM-2 | 87.1 | 11.0 | 0.7 | 1.2 |
| MP-CM-4 | 84.1 | 14.3 | 0.6 | 1.0 |
| MP-CM-6 | 80.2 | 18.6 | 0.3 | 0.9 |

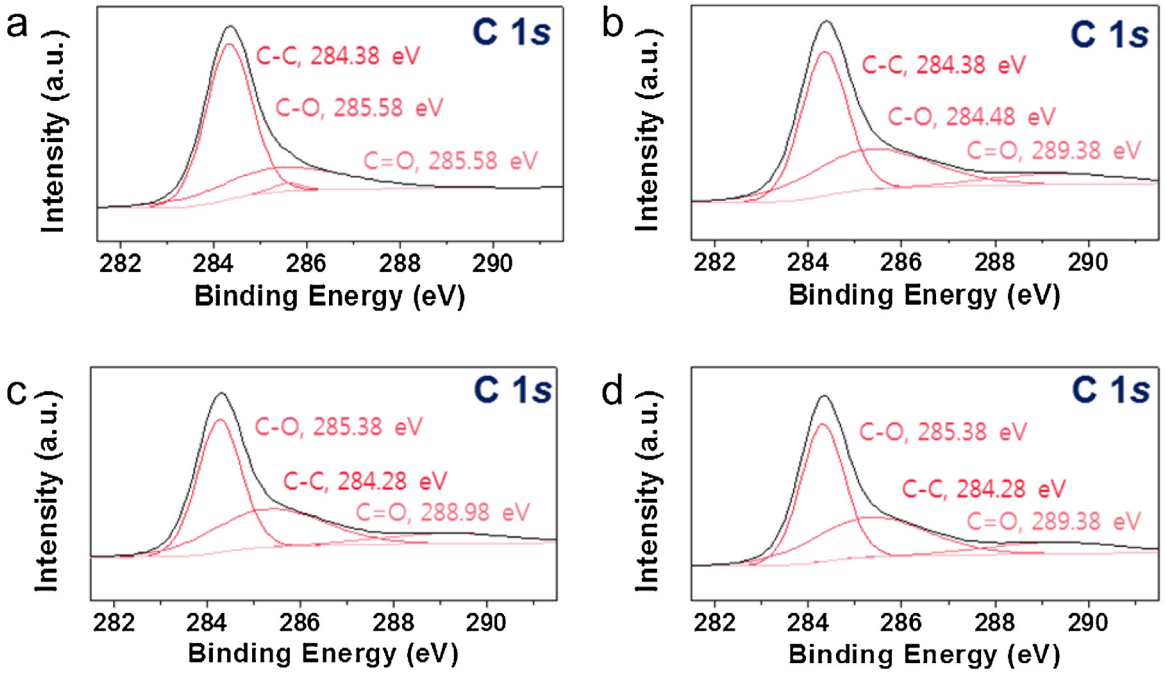


**Fig. 3.** XPS C 1*s* spectra of (a) MP-CM-1, MP-CM-2, MP-CM-4, and MP-CM-6.

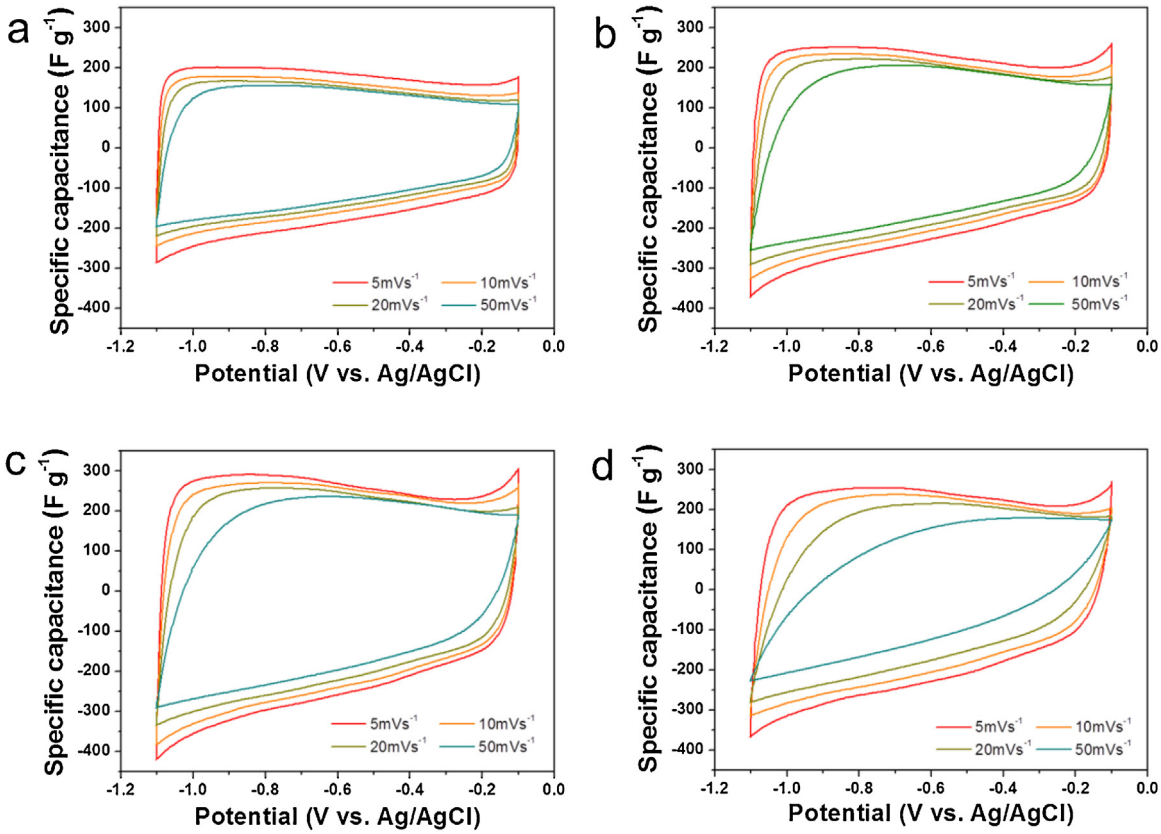


**Fig. 4.** CV curves of (a) MP-CM-1, (b) MP-CM-2, (c) MP-CM-4, and (d) MP-CM-6 at different sweep rates.

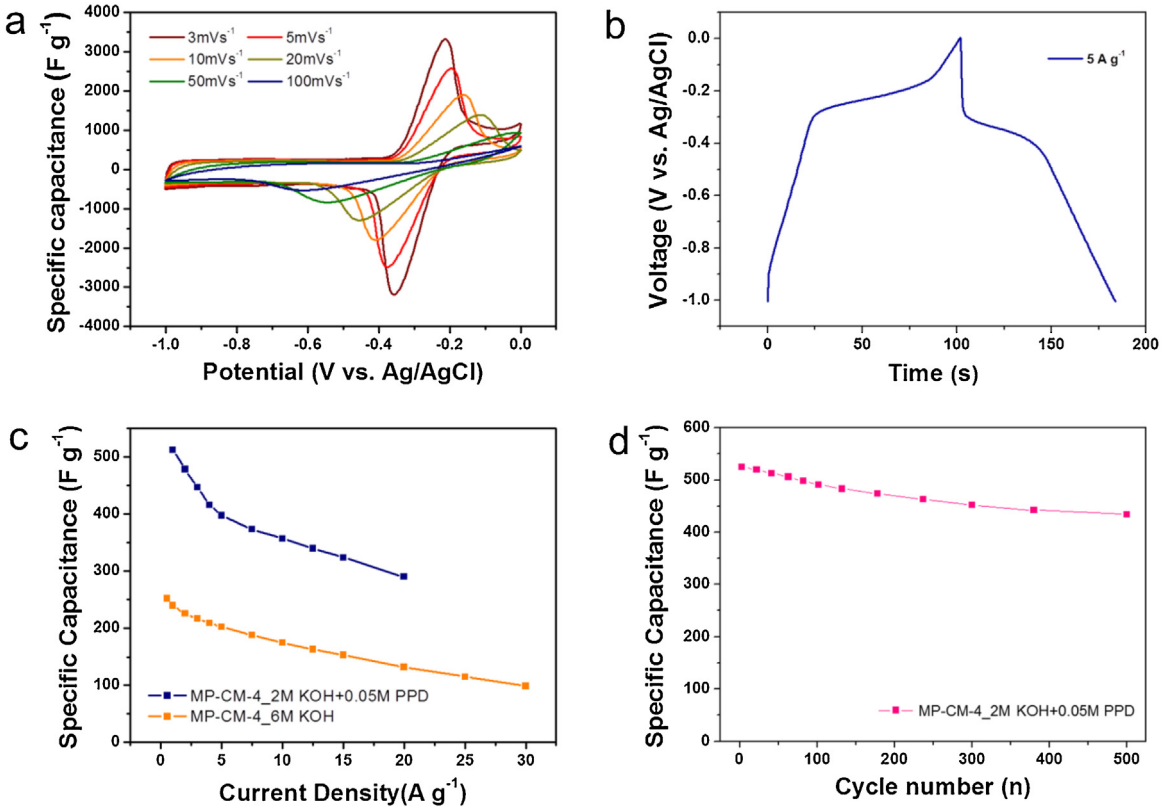


**Fig. 5.** Electrochemical performance of MP-CM-4 in 2 M KOH aqueous electrolyte, including 0.05 M PPD. (a) CV curves at different sweep rates, (b) galvanostatic charge/discharge profiles, (c) comparison of the rate capabilities of MP-CM-4 in the different electrolyte system, and (d) cycling stability over 500 cycles at a sweep rate of 5 A $g^{-1}$.

**Table 3**
Comparison of the specific capacitances of reported carbon-based electrode materials.

| Sample name | SSA[a] | Current density[b] | Specific capacitance[c] | Electrolyte | Ref |
|---|---|---|---|---|---|
| CA-CA-2 | 571 | 0.1 | 220 | 6 M KOH | [7] |
| AC850 | 2,696 | 0.1 | 147 | 6 M KOH | [13] |
| APC 1:4 | 2,960 | 0.1 | 207 | 6 M KOH | [14] |
| AC4 | 1,262.8 | 1.0 | 197.78 | 6 M KOH | [15] |
| C-800-2 | 2587.13 | 1.0 | 502.1 | 6 M KOH in 2.0 mM PNA | [16] |
| C-900-12 | 1,559.1 | 5.0 | 317.6 | 6 M KOH in 12 mM PPD | [17] |
| MP-CMs | 1784.2 | 1.0 | 512 | 2 M KOH in 0.05 M PPD | This work |

[a] Specific surface area ($m^2 g^{-1}$).
[b] ($A g^{-1}$).
[c] ($F g^{-1}$).

in Fig. 2(a). The curves revealed a large amount of nitrogen adsorption in the relative pressure region below 0.05, which originated from the monolayer adsorption of nitrogen molecules on the surface of MP-CMs. In addition, the quantity of nitrogen adsorption is slightly higher at relative pressures above 0.2, indicating that there was no pore filing of nitrogen molecules in the mesopore area ($2 < x < 50$ nm). Therefore, these types of curves are defined as a microporous structure possessing pores mainly <2 nm in size, corresponding to the IUPAC type-I shape [3]. The pore size distribution results of the MP-CMs showed that most pores were less than 3 nm in size, and MP-CM-4 had the highest pore volume in all samples (Fig. 2(b)). The specific surface area and average pore width of MP-CM-4 were 1784.2 $m^2 g^{-1}$ and 3.2 nm, respectively. In addition, the pore volume was 0.88 $cm^3 g^{-1}$. Table 1 provides specific information on the textural properties.

The surface properties of MP-CMs were characterized by XPS (Fig. 3). The XPS C 1*s* spectra of MP-CMs showed similar chemical structures composed of a main $sp^2$ C=C onding and two oxygen functional groups, such as C—O and C=O bonding [24]. The C/O ratios of MP-CM-1, -2, -4, and -6 were 11.0, 7.9, 5.9, and 4.3, respectively, which decreased continuously with increasing contents of activation agents, suggesting that MP-CMs were more activated with increasing content of activation agents. The oxygen heteroatoms can store additional charges by their pseudocapacitive behavior, whereas too much oxygen deteriorates the electrical conductivity of the samples. Therefore, there could be an optimal point exhibiting a pseudocapacitance maintaining good electrical properties. Table 2 lists the specific heteroatom contents of the MP-CMs.

The electrochemical performance of MP-CMs was characterized in 6 M KOH aqueous electrolyte over the potential range between −0.1 and −1.1 V vs. Ag/AgCl. Cyclic voltammetry (CV) curves of the MP-CMs at a sweep rate of 5 mV $s^{-1}$ showed almost rectangular shapes, indicating ideal capacitive charge storage behaviors through EDL formation (Fig. 4). MP-CM-4 had the largest CV area in all samples, indicating it has the highest specific capacitance (Fig. 4(c)). With increasing sweep rate from 5 to 50 mV $s^{-1}$, the rectangular shapes changed gradually. In contrast, the MP-CM-1 maintained their initial rectangular shape (Fig. 4(a)), MP-CM-6 shows a large distortion of the CV shapes that changed to an oval shape at a sweep rate of 50 mV $s^{-1}$ (Fig. 4(d)). The large deformation in the relatively rapid sweep rate indicates poor rate capability, which could be due to the decrease in electrical conductivity by the harsh activation. The specific capacitance was increased significantly using a redox-mediated electrolyte: a 2 M KOH with 0.05 M para-phenylenediamine (PPD) aqueous solution. The CV curve of MP-CM-4 characterized at a sweep rate of 3 mV $s^{-1}$ in the redox mediated electrolyte showed a distinct redox peak at −0.35/−0.21 V, indicating pseudocapacitive charge storage behavior (Fig. 5(a)). In addition, EDLs were observed in the overall voltage range, showing that the charge storage behaviors are based on both pseudocapacitance and EDL capacitance. Through the hybrid charge storage effects, the overall area increased, indicating an increase in specific capacitance. These charge storage manners can also be confirmed in the galvanostatic charge/discharge profiles, as shown in Fig. 5(b). Both the plateau and diagonal regions can be seen distinctively in the profile. The specific capacitance of MP-CM-4 in the redox-mediated electrolyte was 512 F $g^{-1}$ at a sweep rate of 1 A $g^{-1}$, which is much higher than that (252 F $g^{-1}$) in the 6 M KOH aqueous electrolyte. In addition, the specific capacitance of MP-CM-4 was much higher than those of results reported in similar electrolyte systems (Table 3). Although the specific capacitances in the redox-mediated electrolyte decrease with increasing current density, the value was much higher than those in a 6 M KOH electrolyte in the overall current densities. The cycling performance of MP-CM-4 in the redox-mediated electrolyte was tested at a current density of 5 A $g^{-1}$. With repetitive cycling over 500 cycles, stable cycling behavior was observed and approximately 435 F $g^{-1}$ was achieved after the 500th cycle. These results demonstrate the feasibility of MP-CM-4 in the redox mediated electrolyte.

## Conclusion

MP-CM samples were prepared from WCs by heating with different KOH contents. MP-CM-4 showed a high specific surface area of 1784.2 $m^2 g^{-1}$ and numerous nanopores, showing a high charge storage capacity of 252 F $g^{-1}$ and good rate capabilities in a 6 M KOH aqueous electrolyte. The specific capacitance of MP-CM-4 was increased dramatically using a 2 M KOH aqueous electrolyte including 0.05 M PPD. In the redox mediated electrolyte, a specific capacitance of 512 F $g^{-1}$ was achieved at a current rate of 1 A $g^{-1}$ by both pseudocapacitance and EDL capacitance, and stable cycling over 500 cycles was demonstrated.

## Acknowledgments

This study was supported by the Basic Science Research Program through the National Research Foundation of Korea (NRF) funded by the Ministry of Education (NRF-2017R1C1B1004167) and (NRF-2018R1A4A1025169).

## References

[1] P. Simon, Y. Gogotsi, Nat. Mater. 7 (2008) 845.
[2] Y.S. Yun, S.Y. Cho, J. Shim, B.H. Kim, S.-J. Chang, S.J. Baek, et al., Adv. Mater. 25 (2013) 1993.
[3] Y.S. Yun, S. Lee, N.R. Kim, M. Kang, C. Leal, K.-Y. P, et al., J. Power Sources 313 (2016) 142.
[4] H. Jiang, P.S. Lee, C. Li, Energy Environ. Sci. 6 (2013) 41.
[5] K. Xia, Q. Gao, J. Jiang, J. Hu, Carbon 46 (2008) 1718.
[6] Y.S. Yun, M.H. Park, S.J. Hong, M.E. Lee, Y.W. Park, H.-J. Jin, ACS Appl. Mater. Interfaces 7 (2015) 3684.
[7] B.L. Zhao, L.-J. Fan, M.-Q. Zhou, H. Guan, S. Qiao, M. Antonietti, et al., Adv. Mater. 22 (2010) 5202.
[8] B.D. Hylicova-Jurcakova, M. Seredych, G.Q. Lu, T.J. Bandosz, Adv. Funct. Mater. 19 (2009) 438.

[9] H. Ji, X. Zhao, Z. Qiao, J. Jung, Y. Zhu, Y. Lu, et al., Nat. Commun. 5 (2014) 3317.
[10] J. Biener, M. Stadermann, M. Suss, M.A. Worsley, M.M. Biener, K.A. Rose, et al., Energy Environ. Sci. 4 (2011) 656.
[11] J.W.F. To, Z. Chen, H. Yao, J.J. He, K. Kim, H.H. Chou, et al., ACS Cent. Sci. 1 (2015) 68.
[12] Y. Zhang, S. Liu, X. Zheng, X. Wang, Y. Xu, H. Tang, F. Kang, Q.-H. Yang, J. Luo, Adv. Funct. Mater. 27 (2017)1604687.
[13] E.Y.L. Teo, L. Muniandy, E.-P. Ng, F. Adam, A.R. Mohamed, R. Jose, K.F. Chong, Electrochim. Acta 192 (2016) 110.
[14] D.-Y. Lee, G.-H. An, H.-J. Ahn, J. Ind. Eng. Chem. 52 (2017) 121.
[15] E.-S. Cho, B.C. Bai, J.S. Im, C.W. Lee, S. Kim, J. Ind. Eng. Chem. 35 (2016) 341.
[16] Y.Q. Zhu, L. Zhang, X.Y. Chen, Z.H. Xiao, Z.J. Zhang, J. Power Sources 299 (2015) 629.
[17] Z.J. Zhang, X.Y. Chen, J. Electroanal. Chem. 764 (2016) 45.
[18] J. Wu, H. Yu, L. Fan, G. Luo, J. Lin, M. Huang, J. Mater. Chem. 22 (2012) 19025.
[19] S. Roldán, C. Blacno, M. Granda, R. Menéndez, R. Santamaria, Angew. Chem. Int. Ed. 50 (2011) 1699.
[20] H. Yu, L. Fan, J. Wu, Y. Lin, M. Huang, J. Lin, et al., RSC. Adv. 2 (2012) 6736.
[21] H.J. An, N.R. Kim, M.Y. Song, Y.S. Yun, H.-J. Jin, J. Ind. Eng. Chem. 45 (2017) 223.
[22] Z.J. Zhang, Y.Q. Zhu, X.Y. Chen, Y. Cao, Electrochim. Acta 176 (2015) 941.
[23] Y.S. Yun, G. Yoon, K. Kang, H.-J. Jin, Carbon 80 (2014) 246.
[24] M.Y. Song, N.R. Kim, S.Y. Cho, H.-J. Jin, Y.S. Yun, ACS Sustainable Chem. Eng. 5 (2017) 616.